ISSN 2303-4521
Periodicals of Engineering and Natural Sciences *Original Research*
Vol. 11, No. 2, March 2023, pp.22-35

Three-dimensional final element analysis of composite steel - concrete aches

Roaa H. Al-Brees [1,2], Mohamed I. Abu Mahadi [1], Thaar S. Al-Gasham[2, *] Alaa J. Naji[1,3]
[1] Department of Civil Engineering, Academy of Engineering, RUDN University, Moscow, Russia
[2]Civil Engineering Department, College of Engineering, University of Wasit, Iraq
[3]Roads and Transport Engineering Department, University of Al-Qadisiyah, Diwaniyah, Iraq

ABSTRACT

Latest structure construction crafts frequent use of composite steel-concrete arches for building and bridge applications. The leading goal of this research is to describe a three-dimensional finite element model capable of describing the response of a composite steel-concrete arch. The commercial software Abaqus was implemented to develop the proposed approach, where a certain experimental test results in the literature on a scaled steel-concrete composite arch have been compared to validate the accuracy and adequacy of the proposed finite element model. Furthermore, the current research developed a finite element model to study the fundamental behavior of a composite steel box-concrete arch with a specific parameter. These parameters including the degree of curvature, the number of the shear connector, and the support conditions have been considered the main study parameters. The proposed model has presented an excellent prediction of the initial stiffness, the ultimate strength, and the ductility of the composite arch. The Representative behavior was affected significantly by the designated variable for the steel box section with composite deck. Therefore, these findings may be crafted with the aim of structural design rules.

Keywords: Composition Arc, structure steel, Concrete Deck, steel bridges

Corresponding Author:

Roaa H. Al-Brees
Department of Civil Engineering, Academy of Engineering, RUDN University, Moscow, Russia
Civil Engineering Department, College of Engineering, University of Wasit, Iraq
Wasit, Iraq
E-mail: rbstrhk90@gmail.com

1. Introduction

As a consequence of the benefits of the advantages of steel and concrete combining, steel-concrete composite beams are nowadays extensively used for bridge construction and industrial buildings. Specifically, for continuous beams and steel bridges with concrete slabs, in comparison with simply supported schemes. These components have numerous advantages such as seismic resistance, high ultimate strength, reduced displacements, and economic steel weight [1]. Though, the actual desirability of composite construction is founded on the effective connection between these materials giving composite members their unique behavior [2, 3]. The presence of shear connectors in this type of construction that are either griped or welded to the steel joist top surface and embedded during concrete pouring, provides the composite action. Moreover, the sufficient strength and stiffness, which resulted from the interconnection among the concrete and steel components of a composite member, enabled the two components to be designed as a part of a single structure member [4-6]. There are several shapes and types of shear connectors, the most common are grip and the stud shear connector, which consists of a head and a plain shank connected to the steel component by a welded collar. Subsequently, many researchers have inspected different aspects of composite behavior extending from experimental studies to analytical-numerical solutions, where [7, 8] presented a comprehensive review of the state-of-the-art in this field. However, numerous arrangements of the composite steel-concrete section are currently used in structural engineering. The furthermost familiar segment is that of the composite T-section, in which the steel I-section acts as the web and the reinforced concrete slab acts as the compression flange. According to the improvement in the computer program and software technology, it has been a huge amount of interest devoted in the last

decade to three-dimensional finite element modeling. Such models tend to validate against experimental results, in addition to investigating the effects of concrete compressive strength, type of slab deck, and opening in steel beams. Along with the spacing, and diameter of the clearance hole of shear connectors to avoid relying on the experimental data that was achieved by push-out tests. Examples of such contributions include [9-15].

2. Composite arch

An Arch is defined as a curved structure that acts like an inverted cable; it can be used likewise to reduce the bending moment in a long-span structure. It is mainly subjected to compression but because of rigidity, it can resist bending moment and shear force and is restricted. Composite arches can be used for roofs of halls or for bridges, where their strength depends upon the mechanical interaction between two or more materials. Steel arched girders carrying cylindrical decks using shear connectors may be assembled equivalently at ordered distances in the longitudinal direction of a building or tunnel space to form together the roof surface [16-20]. The function of shear connectors is to transfer tangential and normal forces between the concrete slab and the steel arch so that the composite action can be obtained. Aiming at the architectural requirement, geological characteristics, and environmental requirements, most often the term composite arch is applied in building and bridge construction. For example, Zaodu bridge shown in Figure 1 is an arch bridge Crossing the Zaodu River between the Guizhou and Chongqing Provence, which is a vertical rotating steel box–the concrete composite arch bridge newly proposed by [21], as (1). Evidently, the actual structural behavior of such kind of structure needs laboratory model testing to understand its performance under loading conditions. Accordingly, several studies were concerned with the composite steel-concrete arch behavior, particularly the buckling of the steel web and the slip between the concrete layer and the built-up steel section. Besides the type of shear connectors and the method of connection under the effect of different types of loading, such as the studies of [22-26]. Based on the forging, the main aim of this research is to conduct a three-dimensional finite element model capable of describing the response of a composite steel-concrete arch. Furthermore, A parametric study of composite steel box-concrete arch was carried out with specific parameters in order to investigate the representative behavior for this type of section box composite arch construction.

Figure 1. Zaodu Bridge [21]

3. Method

In the last decade, researchers have devoted a huge amount of interest to three-dimensional finite element (FE) models. These models usually represent the component of a composite section in three dimensions, mainly the shear connectors in order to avoid relying on the experimental data found by push-out tests. The commercial software Abaqus CEA was used to simulate the composite arch component (Steel, concrete- reinforcement, and bolts) for the current proposed finite element model. Model geometry formulation, material behavior, element types, and solution technique, are outlined with specified descriptions in the following subsections: -

3.1. Material Modeling

3.1.1. Structure steel, reinforcement, and shear connectors modeling

Figure (2) showed the model assembly that was adopted in modeling the composite arch, where the steel density of all of the components was assumed to be 7800kg/m^3. As is conservative, all the steel parts were modeled as

a plastic model, associated with the plastic flow and isotropic hardening [9]. The Elastic modulus and Poisson's ratio of the shear connector and steel sections were assumed as 200 GPa and 0.3, respectively. The material behaviour of the steel beam was represented by the bilinear stress-strain relationship with a hardening branch as shown in Figure 2. The yield, ultimate stress, and the plastic strain need to be input to define the steel section and the shear connectors were 350, 500, and 0.178. Conversely, an elastic-perfectly plastic model is defined without hardening branch for which 450 MPa represents the yield stress of the steel reinforcement bar.

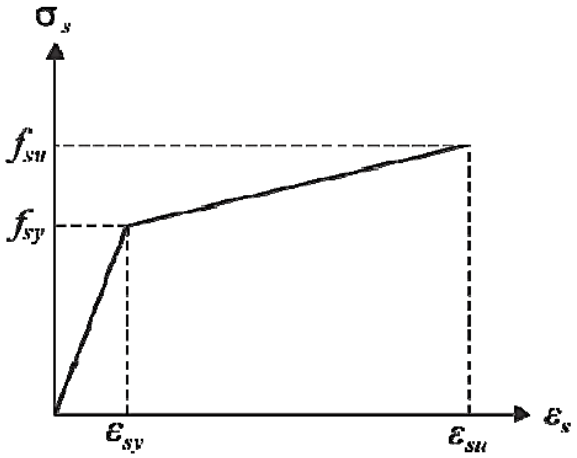

Figure 2. Steel and bolt Material constitutive model

3.1.2. Concrete modeling

The density of the concrete deck for structural computations was assumed to be 2400kg/m^3. The concrete damaged plasticity (CDP) model is a continuum, plasticity-based, damage model for concrete behavior that is governed by two basic failure mechanisms, which are Compressive crushing and tensile cracking [27]. This model assumes that both compressive responses and uniaxial tensile are categorized by plastic damage, as can be seen in Figure (3).

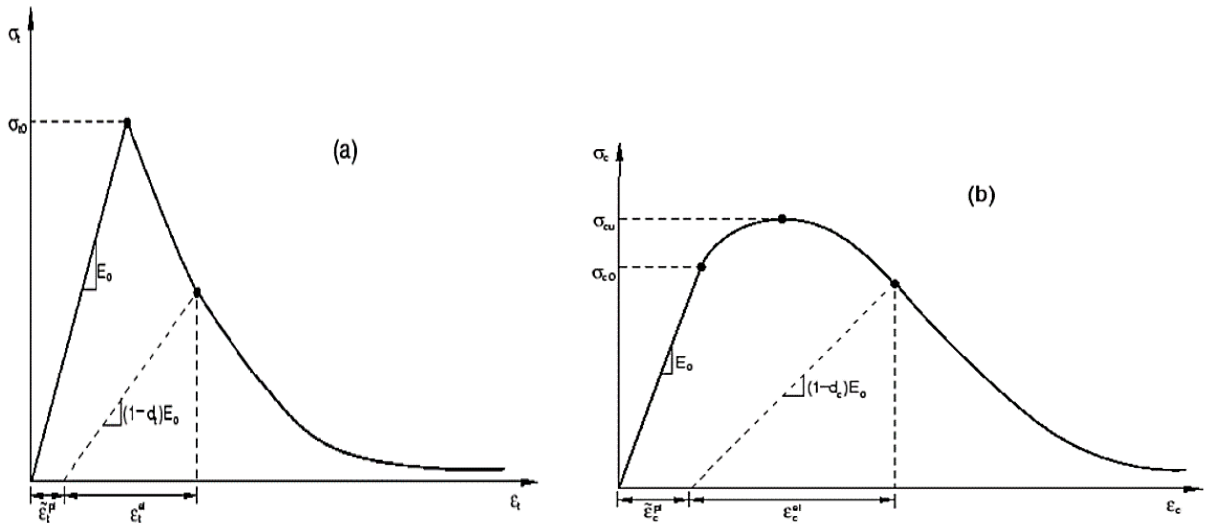

Figure 3. Uniaxial loading response of concrete in tension (a) and compression (b) [28]

Anyhow, the strain and strain data for both compression and tension were obtained from [29]. Then, the other data were deduced from the stress-strain curve shown in Figure 4 using the standard Abaqus CEA formulation.

The damage parameter, cracking, crushing, and inelastic strain were calculated using the Abaqus CAE equation as described above.

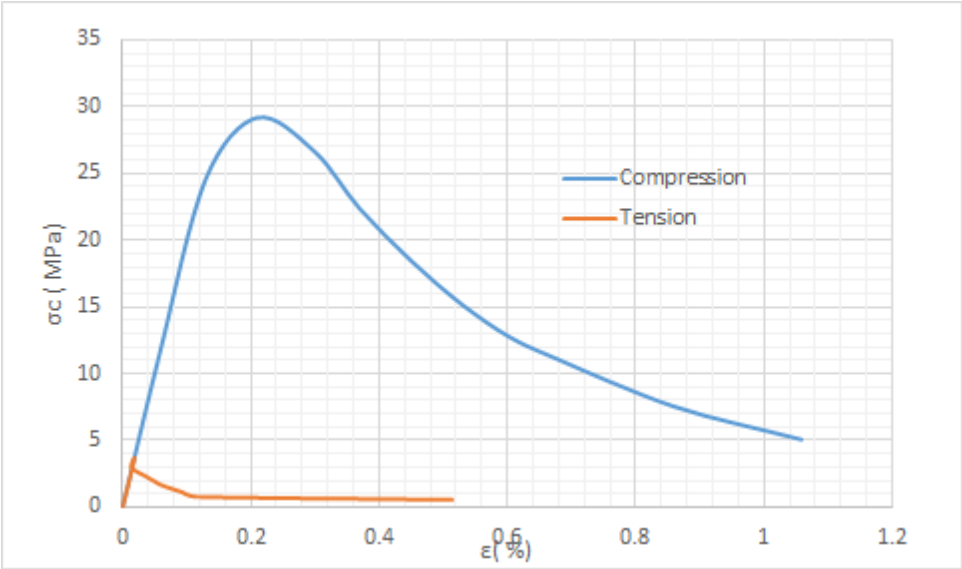

Figure 4. Response of concrete to uniaxial loading data [29]

3.2. Interaction and constraint conditions

Proper interaction and constraint requirements were expressed between the different components, after all, the components of the model were correctly positioned all together in the assembly. The standard interaction (surface-to-surface contact) presented in ABAQUS software was employed at the initial and load step. The penalty contact method at the initial stage, which is complementary to general contact modeling, was chosen as the mechanical constraint formulation, coupled with the normal behavior. The friction coefficient was adopted to specify the penalty option within the tangential response. This coefficient was considered to be 0.6 for the normal interface between the steel and concrete components and 0.3 between steel components (Bradford, n.d.). On the other hand, the tie constraint was applied between the shear connectors and the steel beam. The bottom area of the studs was picked as the master surface, while a surrounding area of the steel box top surface was chosen to represent the slave surface according to their location. Finally, the reinforcing steel bars and shear connectors were constraints with the concrete slab separately due to the different hoist regions using the embedded constraint, while the debonding and relative slip effects of the reinforcement concerning the concrete slabs were ignored.

3.3. Finite element mesh

Figure 5 shows the overviews of the finite element model created in this analysis, alongside the default coordinate system wherein the Y and Z axes state the cross-sectional plane while the X-axis represents the longitudinal arch axis. A Three-dimensional four-node (S4R) quadrilateral, displacement **shell** element with reduced integration was applied for the steel beam. In the same role, three-dimensional (C3D8R) eight-node elements with a linear approximation of displacement, and reduced integration with hourglass control were used for both the shear connector and the concrete deck slab. A three-dimensional truss element (T3D2) of two nodes with linear displacement approximation was considered for steel reinforcement. The region around the shear connectors on the top surfaces was partitioned to achieve accurate results, where a conventional mesh size was applied for the whole member to reduce the computation time. The approximate overall mesh scale was 24 and 16 mm for the deck and box steel arch, and 150, and 25 for the longitudinal and transvers steel bars. However, the minimum mesh scale was around 6 mm for the shear connector.

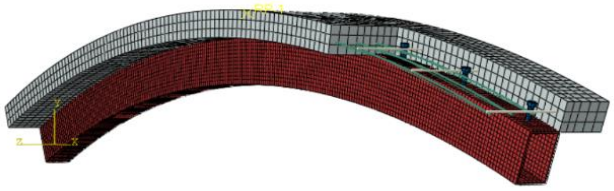

Figure 5. Model mesh

3.4. Boundary conditions

The right and the left end of the steel box section were converted to a rigid body to apply the end support boundary conditions (BC). To complete this BC assignment, a reference point was assigned to the steel box end section for implementing the essential restraints. Elements along the surface of the end of the box section were restrained from translating in the Y directions, as well as rotations concerning the X, Y, and Z-axis for Roller support. Additional restrain was added concerning the translation in Z-axes for the case of Hinge support. Similarly, the Pin support was represented by restraining the displacement in X, Y, and Z directions, respectively, while the fixed support included restraining all the translation and rotational axes. It is worth noting that the assignment of reference points to a rigid body constraint for the right and the left end of the box section causes a slight decrease in the ultimate load capacity of the composite arch. The base of the concrete slab was without any constraint to ensure the concrete uplift and slip. In the same role, rigid body constraints were likewise applied at the center of the concrete deck slab of the composite arch crown to apply the concentrated load.

3.5. Failure Criteria

The feature failure criteria related to the ultimate strength of the different arch components were considered to identify the finite element analysis failure aspects. The failure of the composite analysis in the study was detected by buckling of steel beams, concrete tension damage parameter, and shear connection failure. Steel beam buckling can be clearly captured in ABAQUS, thus it was recognized from the deformed shape of the box section. Then, concrete crushing was outlined once the concrete tension damage parameter reached 0.99, at the maximum cracking strain. Shear connection failure was defined within the ultimate tensile stress that caused a slip of a value between 5, and 7 mm [30].

4. Validation of the developed models

A simply supported composite arch of different support conditions and a number of headed studs tested by [17] have been analyzed, to validate the perfect suitability of the developed finite element model. The results were validated against the corresponding experimental data listed in Table 1. The typical overall shape of the test sections is a segment of a circle (Circular brackets) 2000 mm in length and 200 mm in height measured to the center line of the arched steel girder, as shown in Figure (6).

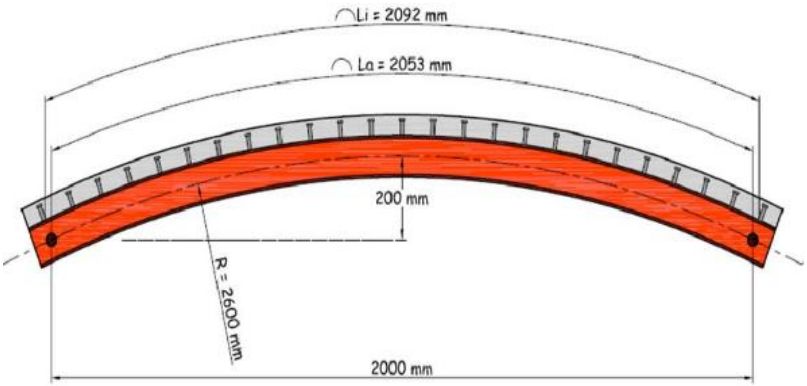

Figure 6. The radius of curvature for the composite steel-concrete arch specimen

One layer of rebars in two of (Ø 4 mm) was used for a 300-width of 50 mm depth concrete slab in the longitudinal tangential direction, the same rebar dimension at a spacing of 110 mm center to center was used in a transverse horizontal direction). The European beam steel girder with parallel-faced flanges IPE100 was formed by curving (bending) about the strong (main) axis to the required curvature as shown in Figure 6, where properties of the selected cross-section properties of IPE100 are given in Table 1. Moreover, the diameter of shear studs was 10 mm with a total length of 38 mm, while the specimen's typical cross-section is shown in Figure 7.

Table 1. Material properties of composite beams [31]

Property	Unit	
Elastic modulus, $\boldsymbol{E_s}$	GPa	200
Yield stress of steel web	MPa	286
Tensile strength of steel web	Mpa	399
Yield stress of flange,	MPa	306
Tensile strength of steel flange	MPa	451
Elastic modulus of concrete, $\boldsymbol{E_c}$	GPa	21
Compressive strength of concrete	MPa	24.88
Tensile Strength Concrete	MPa	2.01
Yield stress of Bolt	MPa	244
Tensile strength of the Bolt,	MPa	274
Friction coefficient at the steel-concrete interface	-	0.6
Yield stress of Reinforcement bar $\emptyset\ 4mm$	MPa	433
Tensile strength of Reinforcement bar $\emptyset\ 4mm$	MPa	

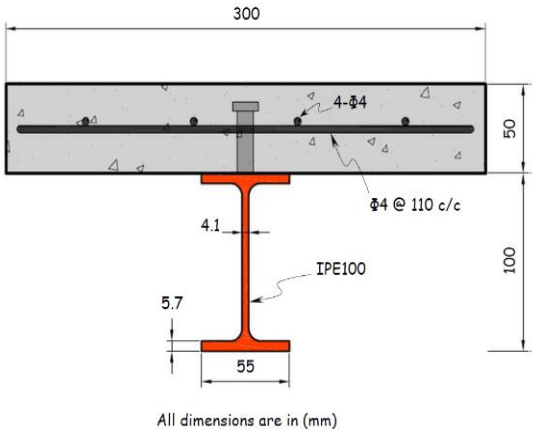

Figure 7. Typical model used for the comparative study

Liner static general analysis was achieved for the composite arch in the experimental study which is (HR11) as the H refers to the Hing support condition and the R refer to the Roller support, and the number 11 represents the number of shear connecter along the arch center. Regarding the experimental result, the material properties, composite arch response, as well as the experimental test findings. An adequate prediction of the initial stiffness, the ultimate strength the ductility of the composite arch was presented in the proposed finite element model shown in Figure 8. Five kN for each loading step was applied separately to record the ultimate load capacity of the finite element analysis, which was (36.5 kN and 75). The ultimate load was 8% less than the experimental one (40 and 80 kN). The insignificant discrepancy in the post-peak load behaviour could be attributed to the asymmetric behavior of the experiment models. Mainly caused by the type of support condition in addition to the un-specified dimension of the I section near the supports at both sides. Along with the sudden rapture of

shear connectors inside the deck slab, which is influenced partially by many uncertain reasons that are unpredictable in the procedure of the experimental program.

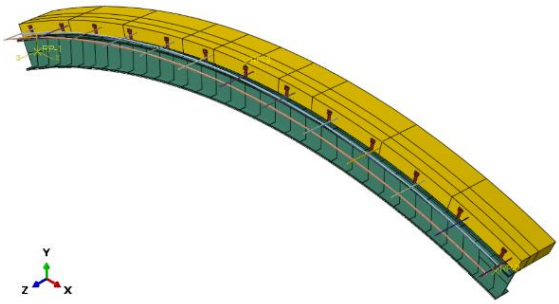

Figure 8. three-dimension model of (HR11) used for the comparative study

However, in Abaqus modeling, the deflection at mid-span before failure presents an excellent matching between the experimental and finite element model as shown in Figures (9 a, b) at the yielding of bolt and steel components. These results are consistent with the Shear stud yield stress that was tested before the experimental procedure, which is 244 MPa and 300 for the shear stud while the I steel beam was within the elastic limit. Therefore, the failure mode was characterized by the yielding of the shear connector, then the concrete crushing. After the ultimate load (38.5) the deflection decreased significantly, based on the linear static analysis in case of an increase in the material properties.

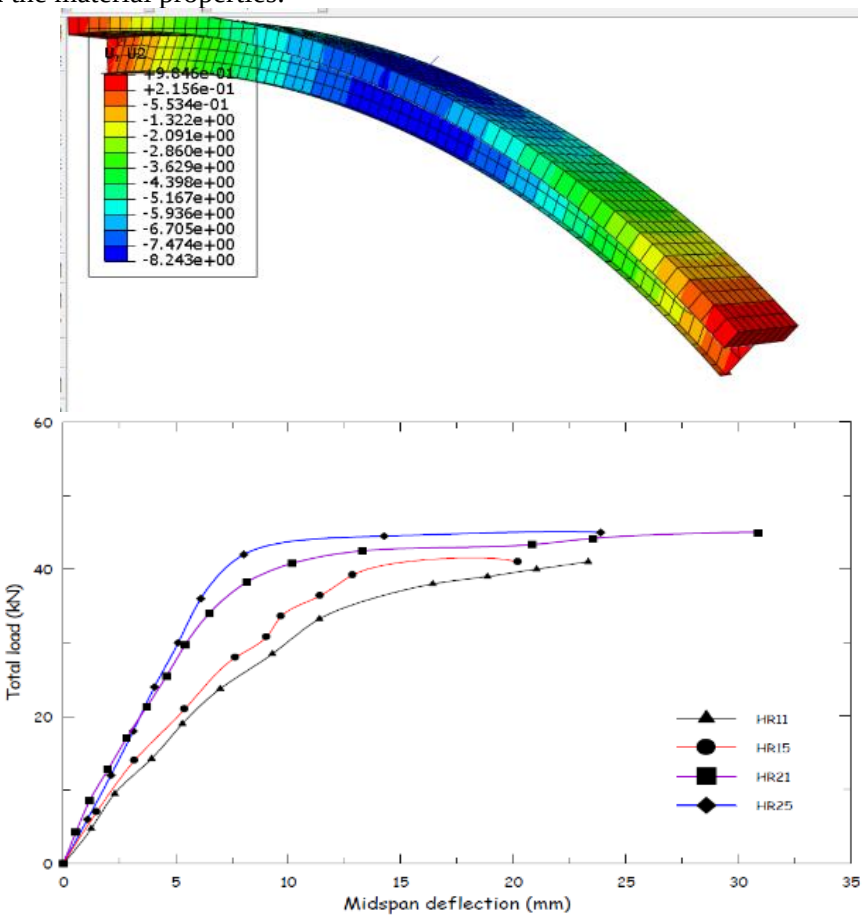

Figure .9 Mid-span deflection at mid-span within the ultimate load of (FE) against HR11 tested by [17]

The low strength of the selected shear stud was considered the main reason for the inadequate composite action for the arch components, where the shear stud yielding resulted in initiating the crack in the concrete deck. As shown in Figure (10-a). The Finite element result showed that the concrete failed at both ends of the concrete

deck as shown in Figure (10-b). The researcher believes that the crack developed at the right and left end, then the crack and concrete crushing of the concrete deck occurred in the mid-span.

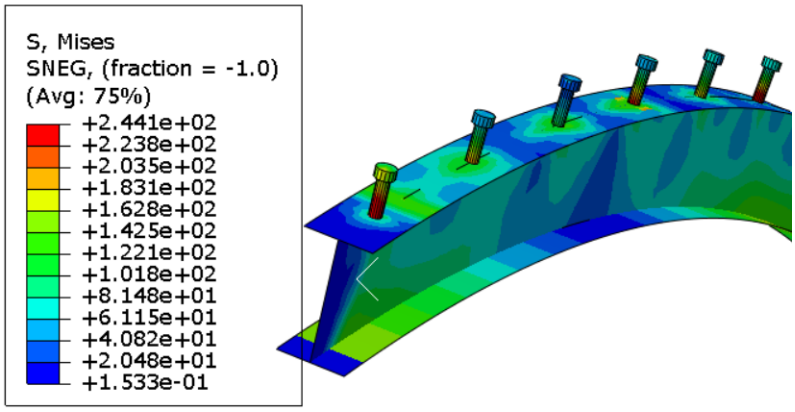

(a) yielding of the shear connector of the HR11 model at 33 kN

(b) longitudinal crack at the right end (Husain et al., 2013)

Figure 10. Failure mode of the tested Model

5. Representative behavior

In order to achieve an optimum representative behavior, in addition, to simplify the current problem. A steel box concrete Arch with a typical shear connector stud was adopted, with a scaled dimension based on the experimental literature mentioned previously. This section aimed to understand the real behavior of composite arch under three main variables, which are the radius of curvature, the number of shear connectors, and the support condition. Figure 11(a) showed a typical cross-section of the composite arch, while the complete composite arch model is shown in. Figure 10 (b) The analytical model was named based on the study parameter, as the (RS) model refers to the radius of the curvature, and S refers to the shear connectors. The height of the arch was (200, 300, and 400 mm) of (2600, 1816.6, and 1450 mm) radius of curvature, respectively, while the number of shear connectors was (13,17, and 22), respectively. The spacing between the shear connector was

applied symmetrically from the center of the arch section. The Boundary conditions were applied subsequently with respect to the study main parameters in order to investigate the effect of restraining the translation and rotational displacement on the failure mode pattern of the composite section.

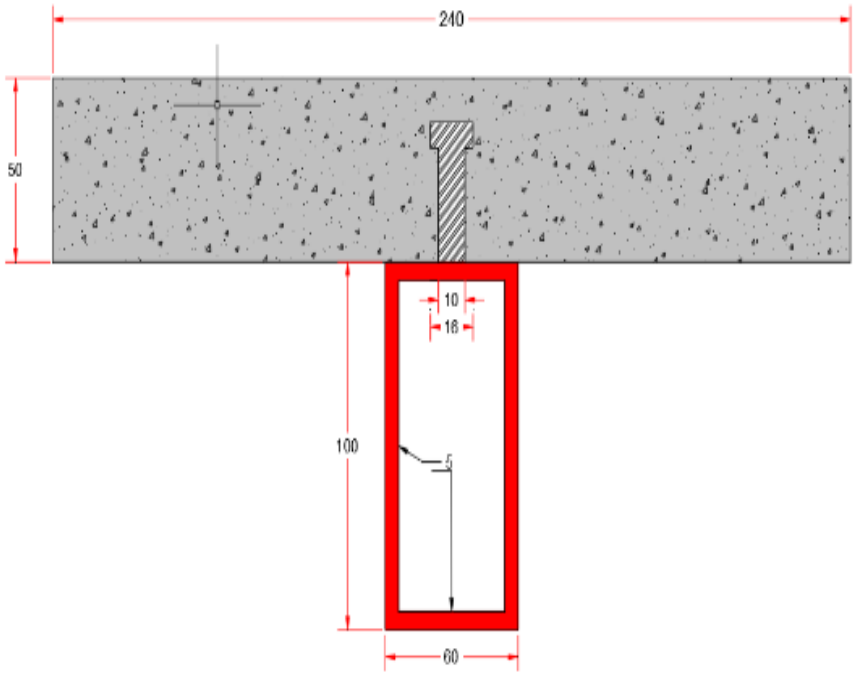

(a) A typical model used for the FE modeling

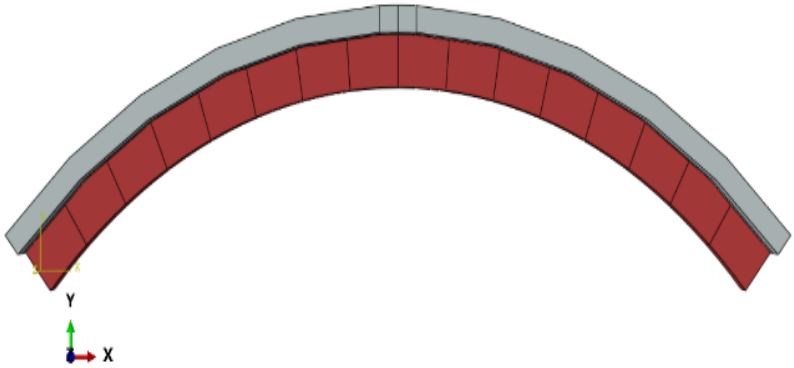

(b) three-dimensional model (S13R3)

Figure 11. Composite arch section and model

6. Results and discussion

6.1. Ultimate load

The finite element models result shows the effect of the degree of curvature on the ultimate load, when the radius of curvature ranges between (2400, 1816, and 1450 mm), the ultimate load capacity increased by (20 and 41.5%) of the ultimate load of the comparison model, respectively according to the proposed material. This increase in ultimate load is due to the increase in the value of axial force and an increase in stiffens of the beam is obtained. In the same role, the ultimate load increase with the increasing number of shear connectors as listed in Figure 12. This behavior is attributed to the increase in the effect of axial force and the decrease in the

movement between steel and concrete. Conversely, the ultimate load also varied significantly with the support condition as illustrated in section 6.3.

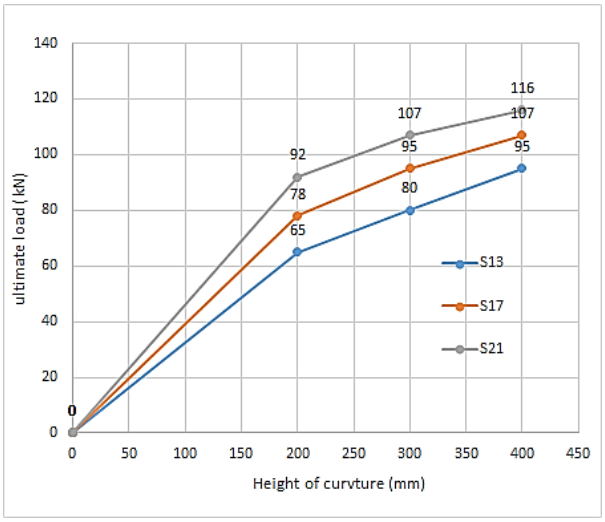

Figure 12. Ultimate load height of curvature curve under the selected boundary condition

6.2. Load–deflection response

The composite arch has increased in ultimate load and deflection due to the increment in its stiffness' and the effect of the axial load as shown in Figure 13.

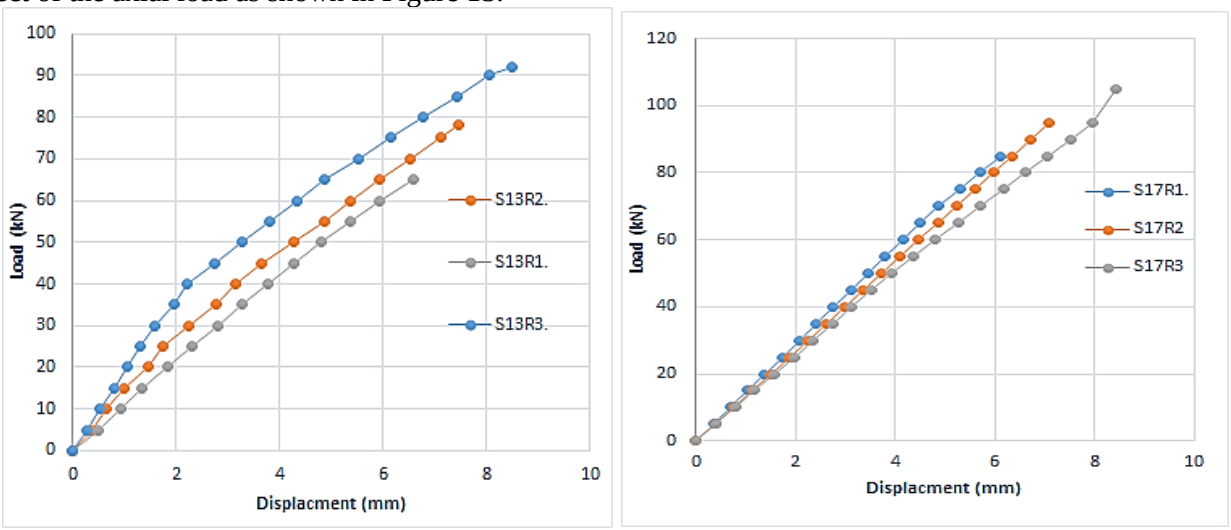

Figure 13. Load deflection curve for the finite element models for se

It can be noted that there is a significant effect of the number of shear connectors that will increase the deflection values significantly due to the increase in the effect of axial force and decrease in the movement between the steel and concrete which increase in deflection value. Moreover, it can be seen that there is a significant effect from the radius of curvature or the height of the chord on the behavior of load-deflection curves. The increase in curvature of the beam will decrease the deflection due to the increased stiffness of the beam and the increase in the effect of axial force. A comparison between the interaction parameters and the load deflection was presented in this section under the effect of Hinge support demonstrated below. Then, the effect of boundary condition on the composite arch will be discussed further in section 6.3.

6.3. Effect of boundary condition

The main study parameters mentioned previously in section 6.1, and 6.2 were achieved under the effect of the assumed boundary condition in section 3.4, where the finite element models are free to translate in the x-direction. the Main reason for specifying these boundary conditions is due to the high rigidity resulting from

Fixed and pined support boundary conditions. Though, the ultimate load capacity is affected significantly by variations in the boundary condition of the composite arch section. In comparison, certain models were selected to show the variation of ultimate load capacity within the different boundary conditions as listed in Table 2. Accordingly, the failure mode would significantly affect the type of selected restraint of composite arch, which will be explained in detail in sections 6.4, and 6.5. The increase in the ultimate load within the Pinned and fixed boundary condition is due to the adequate distribution of stress across the top surface of the steel box section, especially at the end support. These BC provide a massive stiffness for the composite arch which was observed in the deflection values under the loading stage.

Table 2. Effect of the symmetric boundary condition on the ultimate load capacity

Model	Fixed	Pinned	Hing
	Ultimate load capacity		
S13R1	105	85	65
S18R2	143	127	95
S23R3	170	143	116

6.4. The damaged tension in the concrete deck

The first crack developed in the concrete deck slab of the composite arch section was at both ends of the arch under the first shear connector as shown in Figure (14-a). This behavior is attributed to the developed stress at the top flange of the box section due to the restraint of the boundary condition (Translation in x direction). Additional stiffeners are required at both ends for Hinge and Roller support to avoid the earlier failure of the composite arch section. Despite this fact, the main critical section in all the finite element arch models was developed within the range of $0.45f_c'$ within the shear connectors located at 500-700, and 1400-1600 from the arch length. These cracks developed due to the deformed shape that resulted from the axial load effect. Moreover, the damage tension factor was reduced significantly in the case of Fixed and Pined support at the same location and for the different radius of curvature due to the additional restrain resulting from the boundary condition under the same loading condition as shown in Figure (14-b). Additional reinforcement should be applied at this location for specific boundary conditions Besides. The high-strength grip bolt may reduce the developed forces in these areas. Therefore, the failure mode in the simply supported arch was characterized by concrete deck failure. The cracked strain was developed under the shear connectors due to reaching the maximum limit, while the initiated stress and strain in the steel section and shear connector were within the elastic limit. This action increases the slip and uplift effect between the shear connector and the deck slab, which reflects on the composite action between the arch component. High compressive strength of concrete would be recommended in case of applying specific boundary conditions.

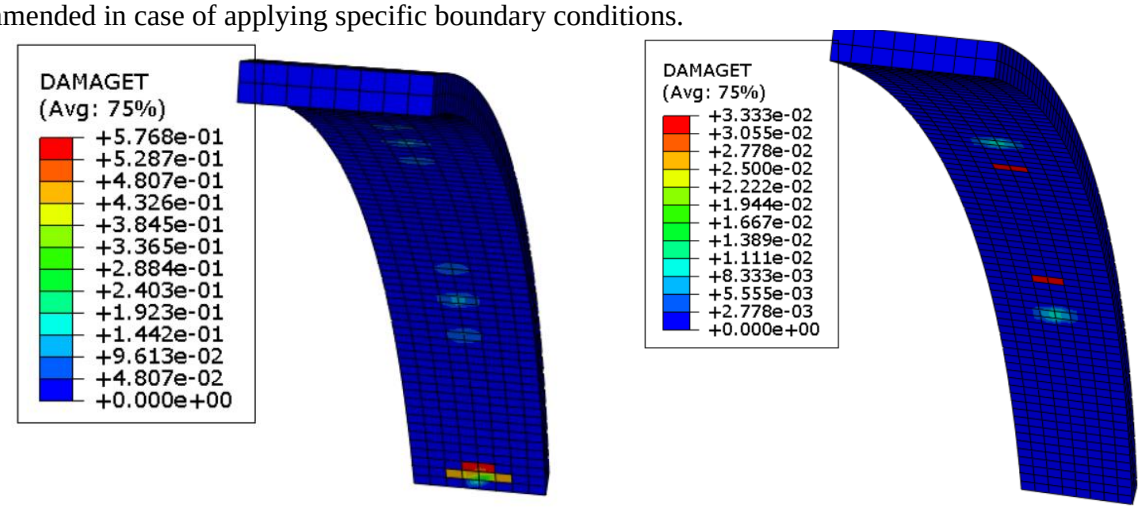

(a) Hinge support (b) fixed support

Figure 14. Concrete damage tension underload of (35 Kn) for S17 R1 Model

6.5. Shear connector's failure mode

Based on the comparison study with the practical results that have already been discussed in section 4. In addition to the similar dimension and modified properties for the shear stud, the stress developed mainly in the connection between the top steel flange and the location previously mentioned in section 6.4 as shown in Figure 15.

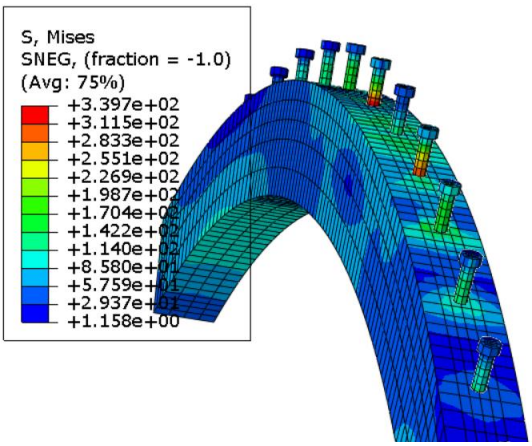

Figure 15. Developed stress in shear connectors under the effect of 110 kN for S17R3 with fixed boundary condition

On the other hand, increasing the number of shear connectors developed the ultimate load capacity due decrease in the movement between the steel and concrete. However, at the yield stage, the bolt rotates, and the inclination of the bolt pushed the concrete out, which resulted in a prying out force that resulted in the pull out of the tied shear connectors. Consequently, this mode of failure caused a failure at the surrounding embedded region due to the yield of removal bolt before the shank yielding as shown in Figures 16 a, and b. It is worth noting that the welding mechanism of the shear connector for composite section construction creates a non-linear behavior. In addition to the theoretical representation by tie constraint to represent the welding area, along with the inclination of the arch resulted in several difficulties in the method of stud's fixation. Finally, the restraint condition reflected on the stud behavior, where any un-restraint in the translation direction applied additional force that causes improper composite action between the box beam and the deck slab

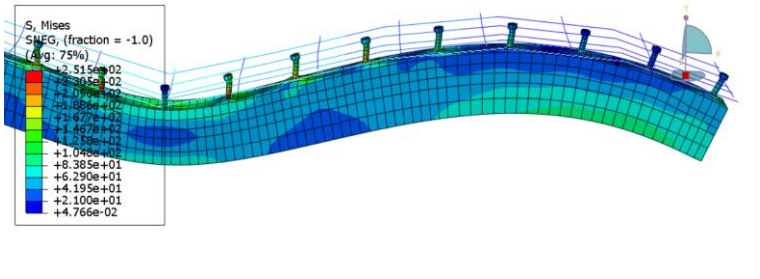

(A) S17 R2 Pinned BC At 100

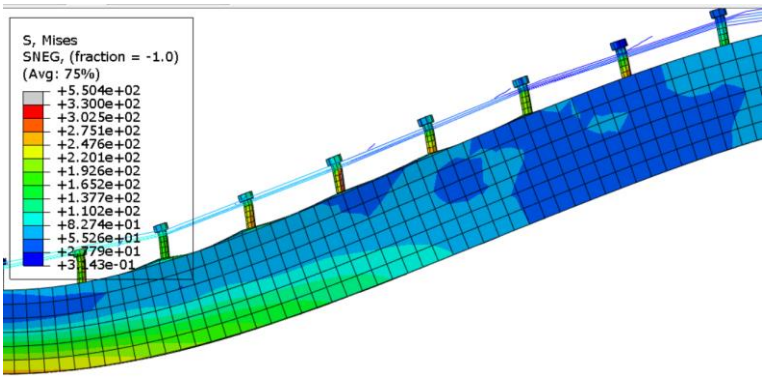

(B) S21 R1 Hing BC at 95 kN

Figure 16. 150 deformation scalE factor for the rotation of the tied shear connector

7. Conclusion

The composite steel-box-concrete arch was affected significantly by the study parameters (boundary condition, height of curvature, and boundary condition). Both the height of the arch and the accurate distribution of the shear connector increased the ultimate load capacity for the proposed finite element model. Otherwise, the boundary condition plays an important role in the failure mode of the arch component, where any un-restraint in both translation and rotation direction creates an additional force that causes inadequate composite action between the arch component. In order to overcome these difficulties or the need to assign a specific boundary condition, high strength grip bolt would be applied, where the box section considers the optimum section for applying this type of connection, compared with the I section. The grip bolt method of connection reduced the effect of non-linearity resulting from the welding process. Furthermore, high-strength concrete would be used to achieve an adequate interaction between the arch components to achieve the optimum composite action

Conflict of interest

The authors declare that they have no conflict of interest, and all of the authors agree to publish this paper under academic ethics.

Author contributions

All the authors contributed equally to the manuscript.

Funding

The work was not supported by any official institute or company.

References

[1] G. Porco, G. Spadea, and R. Zinno, "Finite element analysis and parametric study of steel-concrete composite beams," *Cement and Concrete Composites*, vol. 16, no. 4, pp. 261-272, 1994.

[2] D. Oehlers, D. J. Oehlers, and M. A. Bradford, *Elementary behaviour of composite steel and concrete structural members*. Elsevier, 1999.

[3] P. C. Chiadighikaobi *et al.*, "Performance evaluation of dispersed basalt fiber on strength of lightweight expanded clay concrete," *Cogent Engineering*, vol. 9, no. 1, p. 2137007, 2022.

[4] F. Tahmasebinia and G. Ranzi, "Three-Dimensional FE Modelling of Simply-Supported and Continuous Composite Steel-Concrete Beams," *Procedia engineering*, vol. 14, pp. 434-441, 2011.

[5] S. M. Sargand, I. Khoury, and J. Kurdziel, "A new test method for evaluating the long-term performance of fiber-reinforced concrete pipes," *Advances in Structural Engineering*, vol. 23, no. 7, pp. 1336-1349, 2020.

[6] M. Elshahat, M. A. Mahadi, S. Elroba, N. Dayoub, and L. Petrova, "Effect of fire extinguish methods on RHA-concrete strength," in *Journal of Physics: Conference Series*, 2020, vol. 1687, no. 1: IOP Publishing, p. 012010.

[7] E. Spacone and S. El-Tawil, "Nonlinear analysis of steel-concrete composite structures: State of the art," *Journal of Structural Engineering*, vol. 130, no. 2, pp. 159-168, 2004.

[8] A. Markovich, M. A. Mahadi, S. Gazizova, and D. Miloserdova, "The method of displacements calculating in the joints of timber structures," in *IOP Conference Series: Materials Science and Engineering*, 2019, vol. 675, no. 1: IOP Publishing, p. 012012.

[9] V. Patel, B. Uy, S. Pathirana, S. Wood, M. Singh, and B. Trang, "Finite element analysis of demountable steel-concrete composite beams under static loading," *Advanced Steel Construction*, vol. 14, no. 3, pp. 392-411, 2018.

[10] R. Mutashar, S. M. Sargand, I. Khoury, and M. G. Chorzepa, "Early-Age Deck Cracking from Asymmetric Thermal Behavior in Skewed Adjacent Box Beam Bridges," *Journal of Testing and Evaluation*, vol. 50, no. 2, 2021.

[11] X. Liu, M. A. Bradford, Q.-J. Chen, and H. Ban, "Finite element modelling of steel–concrete composite beams with high-strength friction-grip bolt shear connectors," *Finite Elements in Analysis and Design*, vol. 108, pp. 54-65, 2016.

[12] H. H. Hussein, and S. M. Sargand, *Design proposal for synthetic fiber-reinforced concrete pipes using finite element analysis*. ASTM International, 2020.

[13] A. Markovich, D. Koroteev, M. A. Mahadi, and D. Miloserdova, "Analysis of the theory of calculation of fiber-reinforced concrete with non-steel fibers," in *IOP Conference Series: Materials Science and Engineering*, 2019, vol. 675, no. 1: IOP Publishing, p. 012013.
[14] A. Stasishina and M. I. Abumahadi, "SOME ASPECTS OF RECONSTRUCTION OF FOUNDATIONS," *RUDN Journal of Engineering Research*, no. 2, pp. 82-90, 2016.
[15] N. A. j. Haider Th.Salim Alrikabi, and Mansour S. Farhan, "Design and Implementation of Smart City Applications Based on the Internet of Things," *iJIM*, vol. 15, no. 3, 2021.
[16] I. Khoury, W. K. Hamid, and A. Abdulmohsin Khamees, "Structural Performance of Concrete Corners Reinforced with Different Steel Reinforced Detail under Static Loading," in *Forensic Engineering 2022*, pp. 1109-1120.
[17] H. M. Husain, H. M. Al-Hassani, and A. Y. Zainul-Abideen, "Experimental Investigation of Composite Steel-Concrete Arches," *Engineering and Technology Journal*, vol. 31, no. 13 Part (A) Engineering, 2013.
[18] P. C. Chiadighikaobi, A. A. Muritala, I. A. M. Mohamed, A. A. Abd Noor, E. M. Ibitogbe, and A. M. Niazmand, "Mechanical characteristics of hardened basalt fiber expanded clay concrete cylinders," *Case Studies in Construction Materials*, vol. 17, p. e01368, 2022.
[19] A. Stasishina and A. Mohamed, "ВЫБОР РАЦИОНАЛЬНОГО СПОСОБА РЕКОНСТРУКЦИИ СВАЙНЫХ ФУНДАМЕНТОВ," *RUDN Journal of Engineering Researches*.
[20] A. M. M. Ibrahim and V. Elfimov, "Interaction of a protecting wall with a soil massif in process extractions of Foundation pit," *Вестник Российского университета дружбы народов. Серия: Инженерные исследования,* no. 1, pp. 109-117, 2013.
[21] Z. Zhou, L. Fan, S. Wang, and X. Liao, "Chongqing Wansheng Zaodu bridge—steel box–concrete composite arch bridge," *Structural Engineering International*, vol. 23, no. 1, pp. 71-74, 2013.
[22] I. Mais F., "Experimental study on the behavior of composite steel-concrete arches," *M.Sc thesis, university of Baghdad.*, 2009.
[23] H. H. Hussein, S. M. Sargand, Y. Zhu, and I. Khoury, "Experimental and numerical investigation on optimized ultra-high performance concrete shear key with shear reinforcement bars," in *Structures*, 2022, vol. 40: Elsevier, pp. 403-419.
[24] A. S. Markovich, M. I. A. Mahadi, D. A. Miloserdova, and M. S. Asad, "The stress-strain state of the external wall panel with opening of residential building in case bias," in *AIP Conference Proceedings*, 2022, vol. 2559, no. 1: AIP Publishing LLC, p. 050013.
[25] V. I. Elfimov, D. E. e. Kumerov, and A. M. M. Ibrahim, "The determination of influence of the water-penetraiting layer thickness of the massive dam base-ment for the filtration stream parameters by hydraulic methods," *RUDN Journal of Engineering Research*, no. 1, pp. 23-28, 2013.
[26] M. A. a. Roa'a, I. A. Aljazaery, and S. K. Al_Dulaimi, "Generation of High Dynamic Range for Enhancing the Panorama Environment," *Bulletin of Electrical Engineering and* Informatics, vol. 10, no. 1, 2021.
[27] Z. M. A. Rasoul, "Accuracy of concrete strength prediction behavior in simulating punching shear behavior of flat slab using finite element approach in Abaqus," *Periodicals of Engineering and Natural Sciences*, vol. 7, no. 4, pp. 1933-1949, 2019.
[28] D. Cotsovos and M. Pavlović, "Numerical investigation of concrete subjected to high rates of uniaxial tensile loading," *International journal of impact engineering*, vol. 35, no. 5, pp. 319-335, 2008.
[29] D. G. Lignos, A. R. Hartloper, A. Elkady, G. G. Deierlein, and R. Hamburger, "Proposed updates to the ASCE 41 nonlinear modeling parameters for wide-flange steel columns in support of performance-based seismic engineering," *Journal of Structural Engineering*, vol. 145, no. 9, p. 04019083, 2019.
[30] G. Vasdravellis, B. Uy, E. L. Tan, and B. Kirkland, "The effects of axial tension on the hogging-moment regions of composite beams," *Journal of Constructional Steel Research*, vol. 68, no. 1, pp. 20-33, 2012.
[31] L. Hussein and L. Amleh, "Structural behavior of ultra-high performance fiber reinforced concrete-normal strength concrete or high strength concrete composite members," *Construction and Building Materials*, vol. 93, pp. 1105-1116, 2015.